DIRECT SIMULATIONS OF A LIQUID SHEET IN COMPRESSIBLE GAS ENVIRONMENTS

George A. Siamas
Mechanical Engineering, School of Engineering and Design
Brunel University
Uxbridge, UB8 3PH, United Kingdom
George.Siamas@brunel.ac.uk

Xi Jiang
Mechanical Engineering, School of Engineering and Design
Brunel University
Uxbridge, UB8 3PH, United Kingdom
Xi.Jiang@brunel.ac.uk

Luiz C. Wrobel
Mechanical Engineering, School of Engineering and Design
Brunel University
Uxbridge, UB8 3PH, United Kingdom
Luiz.Wrobel@brunel.ac.uk

ABSTRACT

An Eulerian approach with mixed-fluid treatment was adopted for the investigation of a liquid sheet present at the shear layer of a compressible gas jet. The effects of different topological configuration and surface tension on the flow development have been examined by direct solution of the compressible Navier-Stokes equations using highly-accurate numerical methods. The interface dynamics are captured using volume of fluid and continuum surface force models.

The simulations show that the dispersion of the liquid sheet is dominated by the vortical structures formed at the jet shear layer due to the Kelvin-Helmholtz instability with the axisymmetric case being less vortical than its planar counterpart. It has been identified that the vortical structure development differs between an axisymmetric and a planar configuration. Surface tension affects the flow vorticity and consequently the dispersion of the liquid in the gas environments. In an axisymmetric configuration surface tension tends to promote the vorticity development while in a planar configuration surface tension tends to demote vorticity.

INTRODUCTION

Atomisation during a spray process occurs in a variety of engineering applications such as propulsion and fuel injection in combustion engines. A liquid sheet spray process is a two-phase flow system with a gas, in most cases air, as the continuous phase and a liquid as the dispersed phase in the form of droplets or ligaments. In many applications the gas phase is a high-speed compressible flow while the liquid exhibits by nature incompressibility. The interactions between the two phases, which are coupled through exchange of mass, momentum and energy, can occur in different ways at disparate time involving various fluid dynamic factors. An understanding of the fluid dynamic behaviour of liquid sheets in compressible environments is essential to achieve effective control of the desired transfer rates. Although axisymmetric configuration is used in most commercial atomizers, planar configuration is often employed in academic studies due to its simplicity. It is important to know the extent to which the similarities in the fluid mechanics between the two configurations lie.

Researchers have tried to tackle this complex two-phase flow problem in the past but without taking into account the compressibility effects of the gas phase (Nie, 2001; Klein, 2005; Hou et al., 1997). To date, there is no work reported in the literature with reference to the simulation of a liquid sheet in a compressible gas medium using highly accurate computational tools like direct numerical simulation (DNS).

In this study, a liquid sheet present in the shear layer of a compressible air jet is investigated using an Eulerian approach with mixed-fluid treatment (Crowe, 2006) for the governing equations describing the gas-liquid two-phase flow system, where the gas phase is treated as fully compressible and the liquid phase as incompressible. The effects of different configurations and the effects of surface tension on the flow development of the gas-liquid two-phase flow system are examined by direct solution of the compressible nondimensional Navier-Stokes equations using highly accurate numerical schemes. The interface dynamics are captured using volume of fluid (VOF) (Hirt and Nichols, 1981) and continuum surface force (CSF) (Brackbill et al., 1992) models. The following sections present the governing equations; the numerical methods used; a discussion of the results and the conclusions from a comparative study.

GOVERNING EQUATIONS

The governing equations are based on the fundamental conservation laws of mass, momentum and energy. The flow is assumed to be non-reacting and isothermal and there is no phase change and energy transfer between the two phases. The flow field is governed by the non-dimensional time-dependent Navier-Stokes equations with the gas assumed to be fully compressible and treated as an ideal gas, while the liquid is assumed to be incompressible.

The non-dimensional quantities used in the formulation of the governing equations are: x, streamwise direction; r, radial direction in the axisymmetric case; y, cross-streamwise direction in the planar case; u_x, streamwise velocity; u_r, cross-streamwise (radial) velocity in the axisymmetric case; u_y, cross-streamwise (lateral) velocity in the planar case; t, time; γ, ratio of specific heats of the compressible gas; ρ, gas-liquid mixture density; ρ_g, gas density; ρ_l, liquid density (assumed constant); μ, gas-liquid mixture viscosity; μ_g, gas viscosity; μ_l, liquid viscosity (assumed constant); p, gas pressure; T, temperature; Y, liquid mass fraction; Φ, liquid volume fraction; κ, curvature; σ, surface tension; $E_T = \rho_g\left[e + \left(u^2 + v^2\right)/2\right]$, total energy of the gas with e standing for the internal energy per unit mass ($u = u_x$, $v = u_r$ or $v = u_y$); Ma, Mach number; Pr, Prandtl number; Re, Reynolds number; Sc, Schmidt number; and We, Weber number.

The Eulerian approach used herein assumes that the two phases have the same velocity. The VOF method used in the mathematical formulation has been adapted to account for the gas compressibility. A governing equation for the liquid mass fraction has been solved instead of liquid volume fraction. The relation between the liquid volume fraction and the mass fraction can be derived as

$$\Phi = \frac{\rho_g Y}{\rho_l - (\rho_l - \rho_g) Y} \tag{1}$$

The density and viscosity are considered to be gas-liquid mixture properties and they are functions of the density and viscosity of the individual phases (DeVilliers et al., 2004), which can be given as

$$\rho = \Phi\rho_l + (1-\Phi)\rho_g, \quad \mu = \Phi\mu_l + (1-\Phi)\mu_g \tag{2}$$

The CSF model resolves the surface tension effect as a volumetric force acting in the region where the two phases coexist. This model is very useful since it overcomes the problem of directly computing the surface tension integral that appears in the Navier-Stokes equations, which requires the exact shape and location of the interface. The non-dimensional form of the CSF model is approximated to be $\sigma\kappa/We\,\nabla\Phi$ with the curvature given by

$$\kappa = -\nabla\cdot\left(\frac{1}{|\nabla\Phi|}\nabla\Phi\right) \tag{3}$$

In the mathematical formulation, the governing equations are supplemented by the ideal gas law.

The Axisymmetric Governing Equations

For brevity only the axisymmetric governing equations are presented in the paper. The physical space is spanned by a cylindrical coordinate system (x, r, θ). The conservation laws can be written in non-dimensional form as

$$\frac{\partial \boldsymbol{Q}}{\partial t} = -\frac{\partial \boldsymbol{E}}{\partial x} - \frac{1}{r}\frac{\partial(\boldsymbol{F}r)}{\partial r} - \boldsymbol{G} \tag{4}$$

where the vectors $\boldsymbol{Q}$, $\boldsymbol{E}$, $\boldsymbol{F}$ and $\boldsymbol{G}$ are defined as

$$\boldsymbol{Q} = \begin{pmatrix} \rho_g \\ \rho u_x \\ \rho u_r \\ E_T \\ \rho Y \end{pmatrix} \qquad \boldsymbol{E} = \begin{bmatrix} \rho_g u_x \\ \rho u_x^2 + p - \tau_{xx} \\ \rho u_x u_r - \tau_{xr} \\ (E_T + p)u_x + q_x - u_x\tau_{xx,g} - u_r\tau_{xr,g} \\ \rho u_x Y \end{bmatrix}$$

$$\boldsymbol{F} = \begin{bmatrix} \rho_g u_r \\ \rho u_x u_r - \tau_{xr} \\ \rho u_r^2 + p - \tau_{rr} \\ (E_T + p)u_r + q_r - u_r\tau_{rr,g} - u_x\tau_{xr,g} \\ \rho u_r Y \end{bmatrix}$$

$$\boldsymbol{G} = \begin{pmatrix} 0 \\ -\dfrac{\sigma\kappa}{We}\dfrac{\partial\Phi}{\partial x} \\ \dfrac{-p + \tau_{\theta\theta}}{r} - \dfrac{\sigma\kappa}{We}\dfrac{\partial\Phi}{\partial r} \\ 0 \\ -\dfrac{1}{ReSc}\left\{\dfrac{\partial}{\partial x}\left(\mu\dfrac{\partial Y}{\partial x}\right) + \dfrac{1}{r}\dfrac{\partial}{\partial r}\left[\left(\mu\dfrac{\partial Y}{\partial r}\right)r\right]\right\} \end{pmatrix} \tag{5}$$

where $\tau_{xx}, \tau_{xr}, \tau_{rr}$ and $\tau_{\theta\theta}$ are the constitutive relations for viscous stress components of the gas-liquid mixture and $\tau_{xx,g}, \tau_{xr,g}, \tau_{rr,g}$ for the gas-phase. The gas-phase heat flux components are q_x and q_r.

The liquid mass fraction transport equation takes into account the gas compressibility effects while the effects of mass diffusion are included in the transport of the liquid concentration per unit volume ρY.

To avoid the singularities of the governing equations at the jet centreline, they have been put into a special form, and they are derived from the original equations using l'Hôpital's rule (Jiang and Luo, 2000).

NUMERICAL SCHEMES

The governing equations for both configurations are integrated forward using a fully explicit third-order compact Runge-Kutta scheme (Williamson, 1980). In the DNS the spatial differentiation is performed using a sixth order accurate compact finite difference scheme with spectral like resolution (Lele, 1992). The axisymmetric physical space is spanned by a cylindrical coordinate system while the flow is assumed to be uniform in the azimuthal direction. The planar physical space is spanned by a Cartesian coordinate system.

The high-order finite difference (*Padé*) scheme requires precise definition of the boundary conditions to avoid numerical instabilities, while the boundary conditions must be able to represent the physical conditions as realistically as possible. The computational box has a rectangular shape representing half of the cross-section of the physical problem and has four boundaries: (1) inflow boundary; (2) outflow boundary; (3) symmetry boundary; and (4) far side boundary. The Navier-Stokes characteristic boundary condition (Poinsot and Lele, 1992) is specified at the inlet and allows compatibility with the sixth-order non-dissipative numerical scheme and avoids spurious wave reflections. The local one-dimensional relations (Poinsot and Lele, 1992) have been used to provide compatible relations between the physical boundary conditions and the amplitudes of the characteristic waves crossing the boundary. Non-reflecting characteristic boundary conditions (Thompson, 1987) are used at the outflow and at the far side boundary. The spurious wave reflections from outside the outflow boundary have been controlled using a sponge layer (Jiang and Luo, 2000) which has been proved to be very effective. Symmetry conditions are applied at the jet centerline without any additional characteristic boundary condition.

Roll-up and pairing of the vortical structures are achieved by imposing a small perturbation at the inflow (Sandham, 1994), which has been prescribed in a sinusoidal form with amplitude 1% of the mean flow velocity. The frequencies chosen for the perturbation are the most unstable mode f_0 and its first two leading subharmonics, $f_0/2$ and $f_0/4$. At the inflow, the mass fraction of the thin liquid sheet is specified using a hyperbolic tangent profile, which is located around the jet shear layer $r = 1$ ($y = 1$).

RESULTS AND DISCUSSION

Simulation Details

Four computational cases have been performed in order to investigate the flow characteristics of the gas-liquid two-phase flow, including an idealised axisymmetric case with surface tension, a planar case with surface tension and their corresponding cases without surface tension which has been artificially switched off to isolate its effects. The computational cases are tabulated in Table 1. In all cases, the computational parameters correspond to diesel fuel injection into compressed air at around 15MPa and 300K, where the diesel surface tension is approximately 0.025N/m. The Reynolds number used is $Re = 2000$ which corresponds to a value of 4000 based on the jet nozzle diameter. Optimisation tests for computational domain size, number of grid points, grid distribution and time-step have been performed and therefore the results are considered to be independent of the optimized parameters. For a consistent comparison the number of contours has been kept the same in the plots shown.

Table 1: The computational cases.

Case	Configuration	We
A1	Axisymmetric	240
A2	Axisymmetric	∞
P1	Planar	240
P2	Planar	∞

Instantaneous Flow Structures

Figure 1 shows the instantaneous vorticity contours for all cases at $t = 100$. In the axisymmetric cases only the azimuthal vorticity $\omega_\theta = \partial u_r / \partial x - \partial u_x / \partial r$ has been calculated since it is the only one which is nonzero, while the vorticity shown for the planar cases is $\omega_z = \partial u_y / \partial x - \partial u_x / \partial y$. The vortical structures in the axisymmetric cases are quite large in the streamwise direction and the jet is not widely dispersed in the radial direction. The vortical structures are mainly associated with the external perturbation applied that triggers the Kelvin-Helmholtz instability. The vortical structures in the axisymmetric cases are stretched downstream the computational domain where the flow vorticity is attenuated. The major difference between Cases A1 and P1 is that the vortical structures in Case P1 are larger and more dispersed in the cross-streamwise direction. This is an indication that Case P1 might have undergone more significant vortex interaction and pairing.

In Case A2, where the surface tension has been artificially switched off, it is evident that the flow undergoes a decrease in vorticity and development of vortical structures. On the contrary, the non-existence of surface tension in a planar configuration, shown in Case P2, results in an increase in vorticity development and dispersion throughout the flow field, compared to Case P1. This opposite behaviour of vorticity found in axisymmetric and planar configurations is in good agreement with the findings from linear stability analysis (Sirignano and Mehring, 2000).

The instantaneous streamwise velocity profiles at the jet centreline and shear layer are shown in Figure 2. It can be seen that the streamwise velocity profiles at the jet centreline and at the jet shear layer have the same trend with large peaks and troughs, which indicate that the entire flow

field is dominated by the large-scale vortical structures. The small variations observed in the shear layer streamwise velocity profile are due to the vortex interactions. The axisymmetric without surface tension case, shown in Figure 2(b), follows the trend of Case A1 but there are no large peaks observed in the velocity profile at the shear layer since the non-existence of surface tension demotes vorticity, as it was observed in Figure 1.

The planar cases, shown in Figures 2(c) and 2(d), show increased distances between the velocity peaks and troughs. This is mainly owed to the larger vortical structures found in the flow field compared to the axisymmetric cases. Case P2 shows an increase of the velocity magnitude at the jet centreline at around $x = 13$ compared to Case P1. This is because of the vorticity formation very close to the jet centreline. This vorticity formation is absent in Case P1 since surface tension demotes vorticity in a planar configuration, as it was also noticed in Figure 1.

Figure 3 shows the instantaneous liquid volume fraction contours at $t = 100$. Similar to the vorticity distributions shown in Figure 1, the major difference between the axisymmetric and planar cases is that the liquid shows a larger cross-streamwise dispersion in the planar cases. By comparing Figures 2 and 3 it can be seen that the liquid volume fraction closely follows the distribution of vorticity, which indicates that the liquid sheet is dominated by the strong vortical structures formed at the jet shear layer due to the Kelvin-Helmholtz instability.

In Case A1 the disintegration of the liquid sheet is initiated at around $x = 13$ while there is no disintegration observed in Case A2 where the surface tension is absent. In Case P1 the liquid disintegration occurs at around $x = 7$ while in Case P2 the disintegration is initiated at around $x = 6$. This opposite effect of surface tension on the liquid disintegration between axisymmetric and planar configurations is in good agreement with the vorticity trends observed in Figure 1.

Figure 4 presents the time-averaged streamwise velocity profiles at three downstream locations including the nozzle exit at $x = 0$. In Case A1 it is evident that the velocity profiles show similar "top-hat" profiles, although the jet spreading in the cross-streamwise direction at the downstream locations $x = 5$ and $x = 10$ slightly increases with decreasing maximum velocity. Case A2 shows less increase in spreading in the cross-streamwise direction where the effects of surface tension are not taken into account.

The planar case with surface tension, shown in Figure 4(c), shows an increased cross-streamwise spreading compared to Case A1 especially at the downstream location $x = 10$. This results in a decrease of the maximum velocity at $x = 10$ compared to Case A1. Case P2 shows larger spreading at $x = 5$ and smaller spreading at $x = 10$ compared to Case P1. This is mainly associated with the effects of surface tension on the flow vortical structures that control the mixing and the flow field spreading. The important feature in Figure 4 is that the planar cases have larger spreading in the cross-streamwise direction than the axisymmetric cases. The trends observed are owed to the fact that the axisymmetric cases are less vortical than their planar counterparts and consequently they have a slower mixing with the ambient fluid. Therefore the velocity in the axisymmetric cases spreads less in the cross-streamwise direction and decay slower in the streamwise direction than in the corresponding planar cases.

CONCLUSION

A direct numerical simulation has been performed based on an Eulerian approach with mixed-fluid treatment for the gas-liquid two-phase flow system, where the gas phase has been treated as fully compressible and the liquid phase taken as incompressible. An idealised axisymmetric case and a planar case with identical physical parameters have been examined. Simulations without the presence of surface tension have also been performed in both configurations in order to analyse the effects of surface tension on the flow field. The simulations showed that dispersion of the liquid sheet in a compressible gas jet stream is dominated by the strong vortical structures formed in the jet shear layer due to the Kelvin-Helmholtz instability. The direct comparison between the axisymmetric and the planar cases with surface tension showed that the planar case is more vortical than its axisymmetric counterpart leading to the formation of larger vortical structures.

Surface tension has an opposite effect on the flow development in axisymmetric and planar configurations due to their geometrical differences. In an axisymmetric configuration surface tension demotes vorticity while it promotes vorticity in a planar configuration. The liquid dispersion in the cross-streamwise direction in the planar without surface tension case is increased, since the non-existence of surface tension allows further development of the Kelvin-Helmholtz instability downstream the computational domain. An opposite trend was observed for the axisymmetric without surface tension case, since the non-existence of surface tension does not allow further development of the Kelvin-Helmholtz instability.

The comparative simulations indicate that the effect of surface tension can either attenuate or promote vorticity, depending on the configuration, which subsequently affects the dispersion of the liquid.

REFERENCES

Brackbill, J. U., Kothe, D. B., and Zemach, C., 1992, "A Continuum Method For Modelling Surface Tension", Journal of Computational Physics, Vol. 100, pp. 335-354.

Crowe, T. C., 2006, "Multiphase Flow Handbook", Taylor & Francis, USA.

De Villiers, E., Gosman, A. D., and Weller, H. G., 2004, "Large-Eddy Simulation of Primary Diesel Atomization", SAE 2004-01-0100.

Hirt, C. W., and Nichols, B. D., 1981, "Volume of Fluid (VOF) Method for the Dynamics of Free Boundaries", Journal of Computational Physics, Vol. 39, pp. 201-225.

Hou, T. Y., Lowengrub, J. S., and Shelley, M. J., 1997, "The Long-Time Motion of Vortex Sheets With Surface Tension", Physics of Fluids, Vol. 9, pp. 1933-1954.

Jiang, X., and Luo, K. H., 2000, "Direct Numerical Simulation of the Puffing Phenomenon of an Axisymmetric

Thermal Plume", Theoretical and Computational Fluid Dynamics, Vol. 14, pp. 55-74.

Klein, M., 2005, "Direct Numerical Simulation of a Spatially Developing Water Sheet at Moderate Reynolds Number", International Journal of Heat and Fluid Flow, Vol. 26, pp. 722-732.

Lele, S. K., 1992, "Compact Finite-Difference Schemes With Spectral Like Resolution", Journal of Computational Physics, Vol. 103, pp. 16-42.

Nie, Q., 2001, "The Nonlinear Evolution of Vortex Sheets With Surface Tension in Axisymmetric Flows", Journal of Computational Physics, Vol. 174, pp. 438-459.

Poinsot, T. J., and Lele, S. K., 1992, "Boundary Conditions for Direct Simulations of Compressible Viscous Flows", Journal of Computational Physics, Vol. 101, pp. 104-129.

Sandham, N. D., 1994, "The Effect of Compressibility on Vortex Pairing", Physics of Fluids, Vol. 6, pp. 1063-1072.

Sirignano, W. A., and Mehring, C., 2000, "Review of Theory and Disintegration of Liquid Streams", Progress in Combustion Science, Vol. 26, pp. 609-655.

Thompson, K. W., 1987, "Time Dependent Boundary Conditions for Hyperbolic Systems", Journal of Computational Physics, Vol. 68, pp. 1-24.

Williamson, J. H., 1980, "Low-Storage Runge-Kutta Schemes", Journal of Computational Physics, Vol. 35, pp. 48-56.

FIGURES

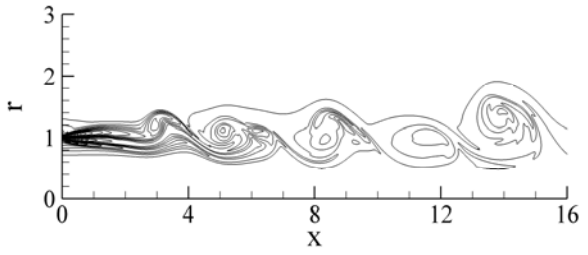

(a) Case A1

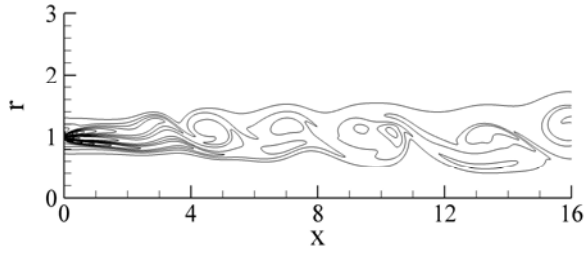

(b) Case A2

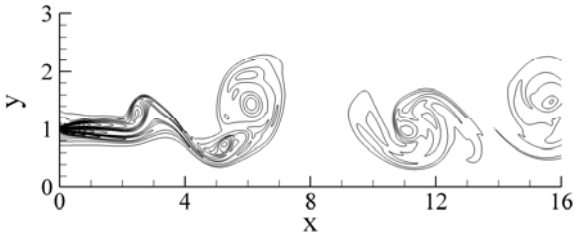

(c) Case P1

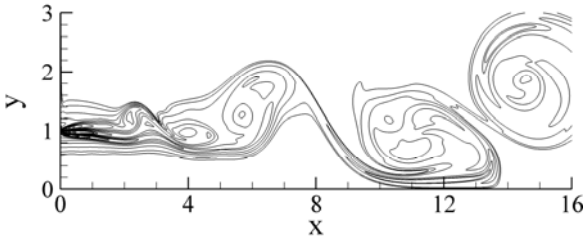

(d) Case P2

Figure 1: Instantaneous vorticity contours at $t = 100$.

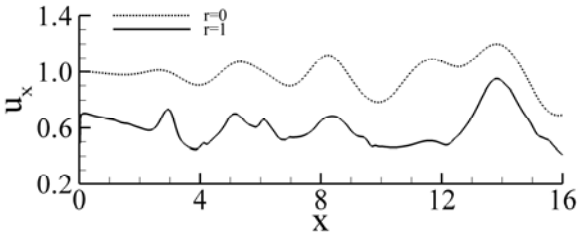

(a) Case A1

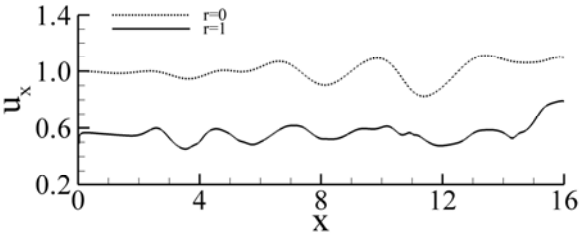

(b) Case A2

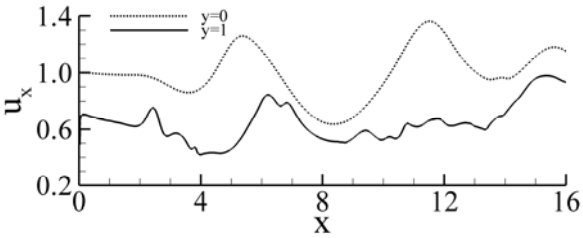

(c) Case P1

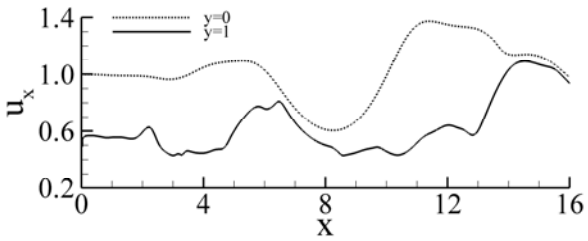

(d) Case P2

Figure 2: Instantaneous streamwise velocity profiles at the jet centreline $r = 0$ $(y = 0)$ and shear layer $r = 1$ $(y = 1)$ at $t = 100$.

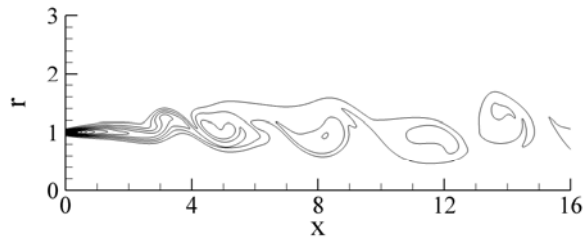

(a) Case A1

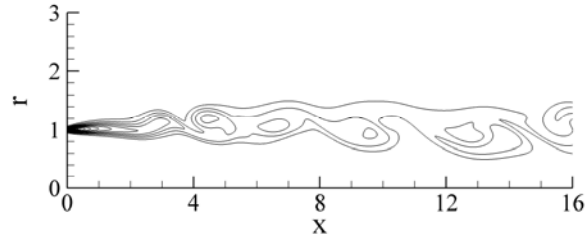

(b) Case A2

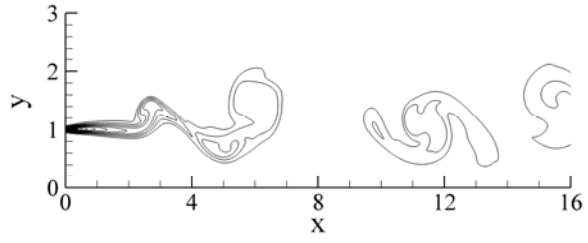

(c) Case P1

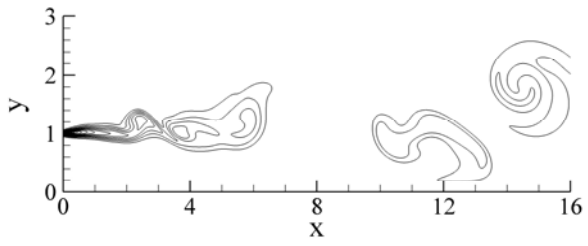

(d) Case P2

Figure 3: Instantaneous liquid volume fraction contours at $t = 100$.

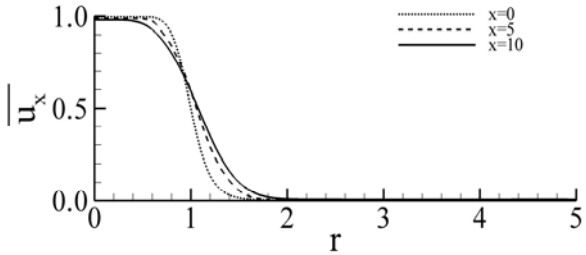

(a) Case A1

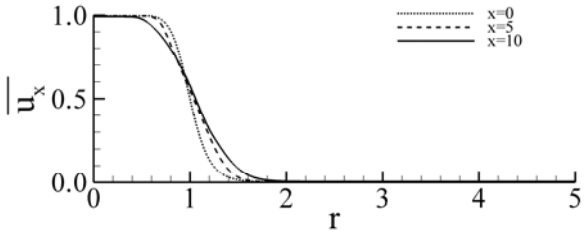

(b) Case A2

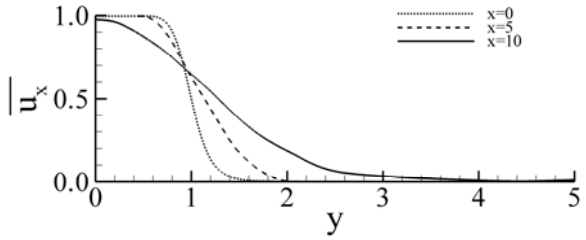

(c) Case P1

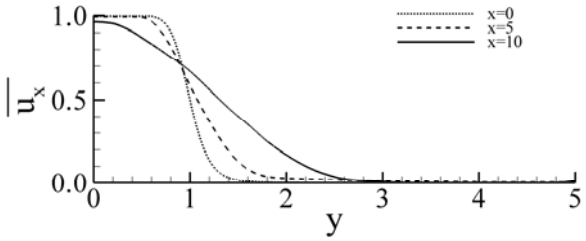

(d) Case P2

Figure 4: Time-averaged streamwise velocity profiles at different cross-streamwise locations.